This is the accepted manuscript made available via CHORUS. The article has been published as:

Exploratory study of fission product yields of neutron-induced fission of ^{235}U, ^{238}U, and ^{239}Pu at 8.9 MeV

C. Bhatia, B. F. Fallin, M. E. Gooden, C. R. Howell, J. H. Kelley, W. Tornow, C. W. Arnold, E. Bond, T. A. Bredeweg, M. M. Fowler, W. Moody, R. S. Rundberg, G. Y. Rusev, D. J. Vieira, J. B. Wilhelmy, J. A. Becker, R. Macri, C. Ryan, S. A. Sheets, M. A. Stoyer, and A. P. Tonchev

Phys. Rev. C **91**, 064604 — Published 5 June 2015

DOI: 10.1103/PhysRevC.91.064604

Exploratory study of fission product yields of neutron-induced fission of ^{235}U, ^{238}U and ^{239}Pu at 8.9 MeV

C. Bhatia[a,b*], B.F. Fallin[a,b], M.E. Gooden[b,c'], C.R. Howell[a,b], J.H. Kelley[b,c], W. Tornow[a,b], C. W. Arnold[d], E. Bond[d], T. A. Bredeweg[d], M.M. Fowler[d], W. Moody[d], R.S. Rundberg[d], G.Y. Rusev[d], D.J. Vieira[d], J.B. Wilhelmy[d], J.A. Becker[e], R. Macri[e], C. Ryan[e], S.A. Sheets[e], M.A. Stoyer[e] and A.P. Tonchev[e]

[a]*Department of Physics, Duke University, Durham, North Carolina 27708, USA*
[b]*Triangle Universities Nuclear Laboratory, Durham, North Carolina 27708, USA*
[c]*Department of Physics, North Carolina State University, Raleigh, North Carolina 27695, USA*
[d]*Los Alamos National Laboratory, Los Alamos, New Mexico 87545, USA*
[e]*Lawrence Livermore National Laboratory, Livermore, California 94550, USA*
** email: chitra@tunl.duke.edu*

PACS number(s): – 25.85.Ec, 24.75.+i, 25.85.-w, 29.30.Kv, 25.40.Fq

Using dual-fission chambers each loaded with a thick (200-400 mg/cm^2) actinide target of ^{235,238}U or ^{239}Pu and two thin (~10-100 μg/cm^2) reference foils of the same actinide, the cumulative yields of fission products ranging from ^{92}Sr to ^{147}Nd have been measured at E_n=8.9 MeV. The ^{2}H(d,n)^{3}He reaction provided the quasi-monoenergetic neutron beam. The experimental setup and methods used to determine the fission product yield (FPY) are described and results for typically eight high-yield fission products are presented. Our FPYs for ^{235}U(n,f), ^{238}U(n,f) and ^{239}Pu(n,f) at 8.9 MeV are compared with the existing data below 8 MeV from Glendenin *et al*., Nagy *et al*., Gindler *et al*., and those of Mac Innes *et al*. and Laurec *et al*. at 14.5 MeV and 14.7 MeV, respectively. This comparison indicates a negative slope for the energy dependence of most fission product yields obtained from ^{235}U and ^{239}Pu, while for ^{238}U the slope issue remains unsettled.

I. INTRODUCTION

Although nuclear fission was discovered more than 75 years ago [1], the experimental study and theoretical understanding of this truly phenomenal process is still far from being complete. The Fission Product Yields (FPY) are one of the most utilized observables of fission. Although gross features dealing with the double peaked structure of the mass yield curve are interpreted within the context of fission theory [2], the yields of individual products and their dependence on the excitation energy of the fissioning system remains poorly understood. This information is of importance for not only a better understanding of the fission process, but also for a number of applied processes including nuclear reactors, nuclear forensics and weapons physics. There have been many FPY measurements over the decades. However, obtaining precise information, especially over a wide energy range, has been elusive.

**McMaster University, Hamilton, L8S2N9, Canada*
'Los Alamos National Laboratory, Los Alamos, New Mexico 87545, USA

To address the FPY issue we are performing a systematic program to resolve long standing differences in various data sets and to establish credible energy dependences of specific relevant fission products. Our goal is to perform a thorough, high precision, self-consistent study that will provide accurate relative information on the energy dependence of FPYs covering the energy range from $E_{th}<E_n<16$ MeV. We intend to accomplish this by minimizing changes in the irradiation and counting configurations used in the experiments performed at different energies - thus eliminating many sources of experimental error. We will couple the results obtained with a modern theoretical analysis to provide a more fundamental understanding of the fission process.

This paper presents an exploratory investigation of this process done with fission induced by 8.9 MeV neutrons on ^{235,238}U and ^{239}Pu and outlines the procedures utilized to extract the relevant data.

II. EXPERIMENTAL OVERVIEW

A schematic of the experimental setup is shown in Fig. 1. It consists of a deuterium filled cell which is separated from the accelerator vacuum by a Havar foil. The incident deuteron beam passes through the Havar foil and the deuterium gas before being stopped in a tantalum beam stop. Quasi-monoenergetic neutrons are produced via the ^{2}H(d,n)^{3}He reaction. A dual-fission chamber is located in close proximity of the deuterium gas cell. The dual fission chamber houses in its center the actinide target of interest, with two thin reference foils of the same actinide placed upstream and downstream of the target in separate ionization chambers. These ionization chambers are used to accurately determine the number of fissions in the thick actinide target in the center of the chamber by taking the mass ratio of the thin and thick targets. In addition, a liquid scintillator based neutron detector was positioned about 3 m further downstream to monitor the neutron flux, and to measure the neutron energy spectrum in auxiliary measurements performed with pulsed incident deuterons.

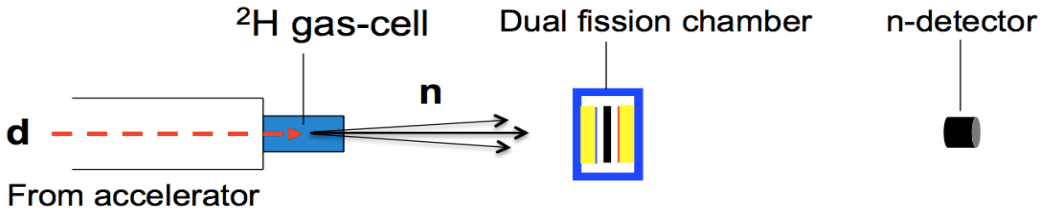

FIG. 1. (Color online) Schematics of experimental ^{2}H(d,n)^{3}He setup using a dual-fission-chamber detector and a neutron detector.

After activation, the actinide target is removed from the dual-fission chamber and inserted into a sealed low-mass cylindrical container made of aluminum. This container is then placed in front of a High-Purity Germanium (HPGe) detector to measure the induced γ-ray activity. This activity is used to identify and track the fission products of interest over a time span of typically six to eight weeks.

II. A. Neutron Production

An unpulsed 2 μA deuteron beam of energy 6.40 MeV was provided by the High-Voltage Engineering Model FN Tandem Van de Graaff accelerator at the Triangle Universities Nuclear Laboratory (TUNL). After passing through a 6.5 μm Havar foil, which separates the beam line vacuum from the gas cell, the resulting 6.0 MeV deuteron beam enters a 3.0 cm long cell filled with 6.9 atm of high-purity deuterium gas. In traversing the gas cell the deuterium beam loses ~ 0.53 MeV in the gas and is then stopped in a 0.3 mm thick tantalum disk at the end of the gas cell. The inner surface of the 1 cm diameter gas cell is also lined with tantalum. A schematic of the deuterium gas cell is shown in Fig. 4(b) of [3]. The resulting neutron beam from the $^{2}H(d,n)^{3}He$ reaction at 0° has a calculated mean energy of 9.00 MeV with an energy spread of 0.54 MeV (FWHM). However, in addition to these monoenergetic neutrons there are also small components of lower energy neutrons. These neutrons are referred to as off-energy neutrons and are described in [3].

Using a sufficiently long flight path the monoenergetic neutron energy spectrum and its off-energy contribution can be determined accurately via a neutron time-of-flight measurement with a well shielded and collimated neutron detector having a very low energy threshold and known detection efficiency. An unshielded neutron detector, as schematically shown in Fig. 1, overestimates the off-energy neutron contribution considerably due to room-return neutrons striking the neutron detector. These room return neutrons cannot always be distinguished from the off-energy neutrons of interest. The relative contribution of room-return neutrons to the monoenergetic and off-energy neutrons at the location of the dual-fission chamber is very substantially smaller than at the position of the neutron monitor [3].

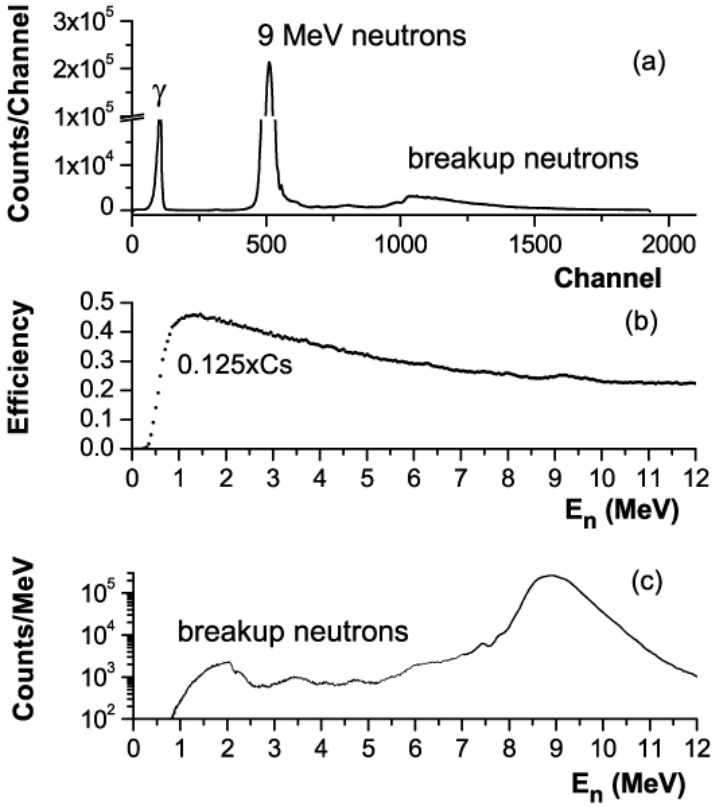

FIG. 2. (a) (Color online) Time-of-flight spectrum for 9.0 MeV neutrons, (b) neutron-detection efficiency and (c) the neutron-yield distribution (logarithmic scale) as a function of energy. See text for details.

A neutron time-of-flight (TOF) spectrum obtained with a pulsed deuteron beam and using TUNL's so-called 4 m neutron detector [4] positioned at 0˚and 3.87 m from the end of the deuterium gas cell is shown in Fig. 2 (a). Time increases from left to right. From the knowledge of the time calibration (0.1955 ns/channel) and the location of the γ-ray flash (1st peak on the left side of Fig. 2 (a), the neutron energy can be calculated from the channel number (~500) of the peak associated with monoenergetic neutrons. This procedure resulted in deduced neutron energy of 9.0 MeV, as designed. The prompt γ rays, which are predominately produced in the Havar entrance foil and the tantalum beam stop of the deuterium gas cell, provide also an accurate measure of the intrinsic time resolution (3.2 ns FWHM) of the present TOF measurement. The first off-energy component referred to above is due to neutrons created in the breakup of deuterons on the Havar foil and the tantalum beamstop. The former produces neutrons with energy between zero and 4.2 MeV, while the latter provides a maximum neutron energy of 3.3 MeV. The second off-energy component is due to deuteron breakup in the deuterium gas itself, resulting in a maximum neutron energy of 1.6 MeV.

The detection threshold of this heavily shielded NE218 liquid scintillator of 8.9 cm diameter and 5.08 cm thickness was set to 0.125 times the channel number associated with the pulse height of the Compton edge of ^{137}Cs (477 keV electron energy), resulting in a neutron energy threshold of approximately 300 keV. Using the known neutron detection efficiency (Fig. 2 (b)), the neutron TOF spectrum of Fig. 2(a) was converted into a neutron energy spectrum (see Fig. 2 (c)). Here, the instrumental time resolution was not corrected for, resulting in a too broad energy distribution of the monoenergetic peak at 9.0 MeV. Correcting for the finite time resolution gives a FWHM neutron energy spread of approximately 0.55 MeV, in agreement with the calculations. As stated above, the off-energy neutron contributions from the deuteron breakup reactions visible in Fig. 2 (c) start at 4.2 MeV and extend to lower energies. The broad enhancement centered at around 6 MeV and the peak at 4.75 MeV are due to the ^{12}C(d,n)^{13}N and ^{16}O(d,n)^{17}F reactions, respectively. The source of the structure at 7.5 MeV has not been positively identified. The neutron detection efficiency curve given in Fig. 2 (b) was calculated with the code NEFF7 [5]. The accuracy of this code has been verified in extensive experimental work (see Ref. [6] and references therein), and was found to be approximately ±3%. From the energy spectrum shown in Fig. 2 (c), the off-energy neutron yield in the 0.3 to 7 MeV energy range was found to be (1.6 ± 0.2)% of the 9.0 MeV monoenergetic neutron yield.

Tests with the deuterium gas pumped out showed that (d,n) stripping reactions on the structural materials of the deuterium gas cell provide a negligible contribution to the yield of interest.

II. B. Dual-Fission Chamber

The three identical dual-fission chambers used in the present work are described in detail in ref. [3]. They were each dedicated to one of the three actinides of interest. The center position of each chamber contained a 1.27 cm diameter activation foil with mass of 0.22 g, 0.42 g and 0.23 g for ^{235}U, ^{238}U and ^{239}Pu, respectively. More details, including the isotopic compositions, are given in Table I. The thin reference foils used in the ionization chamber are of the same actinide material as the thick activation foil, and also have diameters of 1.27 cm. Their thicknesses are ~100 μg/cm^2 for ^{235}U and ^{238}U, ~ 10 μg/cm^2 for ^{239}Pu. Details are given in Table II. As described in Sec. 3.1, the use of the same isotope for the activation and reference foils cancels most uncertainties associated with the determination of the number of fissions occurring in the thick foil for each experiment. Most importantly, this procedure eliminates the need of knowing the fission cross section.

Table I. Details of thick uranium and plutonium targets.

Target	Mass (mg)	Diameter (mm)	Isotopic analysis
^{235}U	223.02(2)	12.35(5)	^{235}U: 93.27% (^{234}U: 1.05%, ^{238}U: 5.68%)
^{238}U	441.93(6)	12.42(5)	^{238}U/^{235}U = 3800/1 -> ^{238}U: 99.974%, ^{235}U: 0.026%
^{239}Pu #3	233.0(2)	12.39(5)	^{239}Pu: 98.41 (40)%, ^{240}Pu: 1.58 (40)%, ^{240}Pu: 0.005 (2)%, ^{241}Pu: 0.003 (1)%, ^{242}Pu: 0.003 (1)%, ^{241}Am: 572(36) ppm in ~1955
^{239}Pu #8	233.7(2)	12.40(5)	same as above for ^{239}Pu #3 target.

The distance between the end of the deuterium gas cell and the front side of the dual fission chamber is 2.54 cm, resulting in a distance of 5.02 cm between the center of the gas cell and the activation foil. Using a Monte-Carlo calculation for this finite geometry, including the well-known differential cross section for the ^{2}H(d,n)^{3}He reaction [7], gives a mean neutron energy impinging on the activation foil of 8.94 MeV with a FWHM energy spread of 0.56 MeV, compared to 9.0 MeV and 0.54 MeV at the position of the neutron monitor.

The efficiency (counts/fission) of the dual-fission chambers of the present design was reported to be > 98.5% [8]. As shown in ref. [3], our measurements with a ^{252} Cf source gave an efficiency of 100% with an uncertainty of 2%.

Table II. Characteristics of monitor foils: FC1 and FC2 (downstream and upstream relative to the neutron source).

Target	Mass (μg)	Diameter (mm)	Isotopic Analysis (wt%)
^{235}U FC			

^{235}U # 6 (FC2)	122.0 (2.3)	12.70(5)	^{235}U: 99.835%
^{235}U # 5(FC1)	118.6 (2.3)	12.70(5)	same as above
^{238}U FC			
^{238}U #3 (FC2)	121.9 (2.3)	12.70(5)	^{238}U: 99.9825 (1),^{235}U: 0.01733 (5), ^{234}U: 0.00016 (1)
^{238}U #1 (FC1)	129.4 (2.3)	12.70(5)	same as above
^{239}Pu FC			
^{239}Pu TP2 (FC2)	8.52 (3)	12.70(5)	"Clinton Pu"- ^{239}Pu: 99.9535 (16) ^{240}Pu: 0.0465 (16)
^{239}Pu TP3 (FC1)	9.556 (3)	12.70(5)	same as above

The fission chamber was surrounded by a cylinder made of 0.5 mm thick cadmium to prevent thermal neutrons from fissioning ^{235}U and ^{239}Pu. As has been described in detail in ref.[3], time-of-flight and neutron activation techniques were used to investigate the importance of thermal neutrons on the observable of interest. They show that low-energy neutrons contribute less than 1% to the total number of fissions occurring in the thick target.

II. C. Gamma-ray counting of fission fragments

After a 48 hour neutron irradiation at an incident flux of $8\text{x}10^{6}$ n/cm^{2}s^{-1}, the thick actinide foils were transferred into counting containers and positioned 5.0 cm in front of a 60% (relative efficiency) HPGe detector. Separate detectors were used for the U and Pu foils. These detectors are located at TUNL's Low-Background Counting Facility. They are shielded against environmental background by a 10 cm thick enclosure constructed of lead bricks. In order to reduce the count rate in the HPGe detector in the case of ^{239}Pu (which had a high intrinsic activity), a 0.5 mm thick disk of cadmium was placed into the counting container and another 0.5 mm cadmium foil was attached to the front of the HPGe detector. The absolute efficiency of the HPGe detectors were determined using calibrated γ-ray sources. A typical efficiency curve is shown in Fig. 3. A Canberra GENIE data-acquisition system [9] was used with Canberra 2026 main amplifiers. Dead-time corrections were typically around 1%, except for ^{239}Pu, where the dead time was 11%, essentially independent of any activation. The three actinide targets were carefully γ-ray counted before neutron irradiation to establish the background in the energy regions of interest. To measure and track the induced γ-ray activity of the fission products, the data-acquisition cycles were gradually increased from 0.5 hours during the first day after irradiation to one day after two weeks, and finally to two days after 4 weeks. This counting procedure allowed tracking the half-lives of all the fission products of interest and to determine any γ-ray interference affecting the photopeaks of interest. The time evolution of the 450 to 550 keV region that contains the high-yield fission products ^{140}Ba and ^{147}Nd is shown in Fig. 4. A list of the fission fragments of interest, their half-lives, characteristic γ-ray lines and associated intensities taken from ref. [10] is given in Table III.

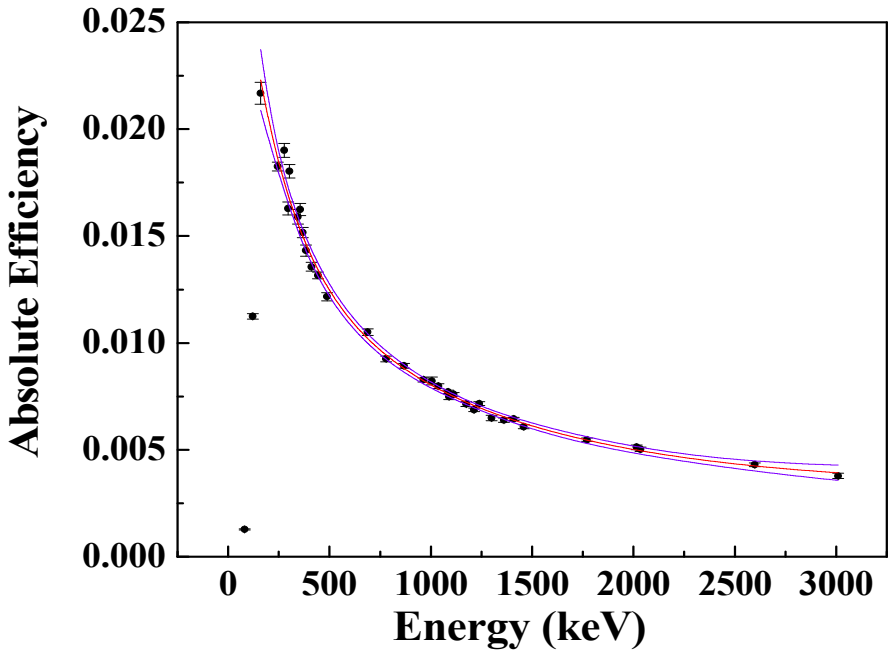

FIG. 3. (Color online) Efficiency of a 60% HPGe detector used for counting the Pu target at 5 cm with a 1 mm cadmium foil absorber. The central dashed curve is the fitted efficiency response for this detector, with the upper and lower curves representing the fit uncertainty.

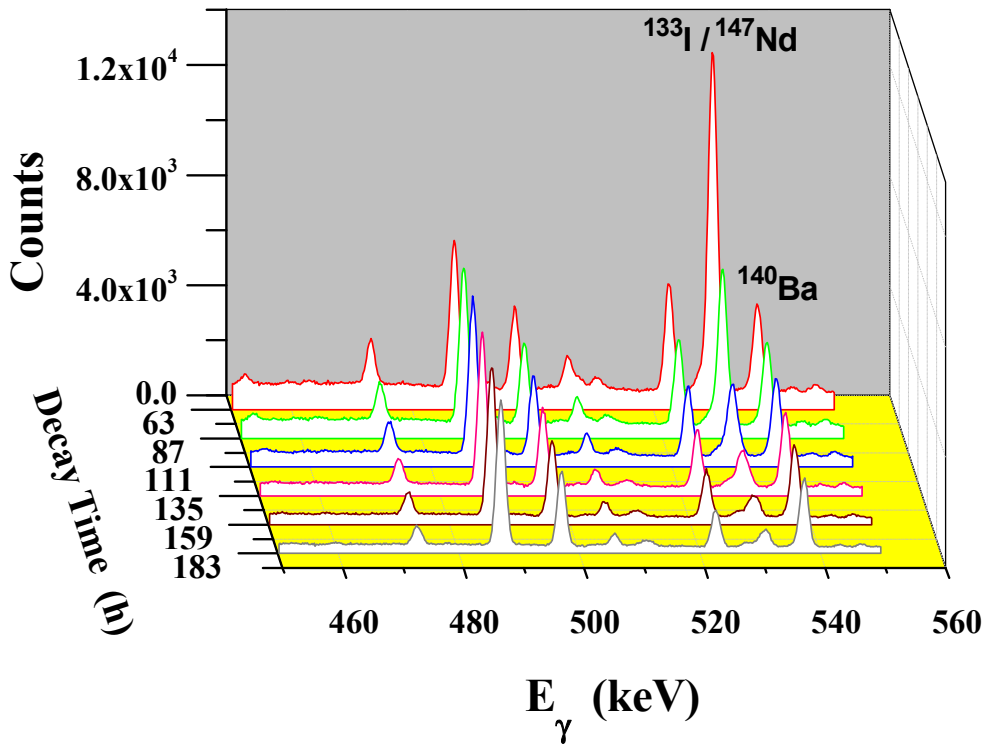

FIG. 4. (Color online) Time evolution of a portion of the gamma-ray spectra emphasizing the region containing transitions from the decay of the ^{133}I and ^{147}Nd "doublet" and the ^{140}Ba fission fragments.

Table III. Characteristics of identified γ-rays.

Fission Fragment	E_γ (keV)	$T_{1/2}$	I_γ (%)
^{92}Sr	1383.93(5)	2.611(17) h	90(6)
^{97}Zr	743.36(*3*)	16.749(8) h	93.09(16)
^{99}Mo	739.500(17)	65.976(24) h	12.26(22)
^{105}Ru	724.30 (3)	4.44(2) h	47.3(?)
^{132}Te	228.16(*6*)	3.204(13) d	88(3)
^{133}I	529.872(*3*)	20.83(8) h	87.0(2.3)
^{140}Ba	537.261(*9*)	12.7527(23) d	24.39(22)
^{143}Ce	293.266(*2*)	33.039(6) h	42.8(4)
^{147}Nd	531.016(*22*)	10.98(1) d	13.37(11)*

* In the literature numbers vary from 2 to 8% [11], and they are different from the present ENDF/B-VII.1 evaluation [10].

In complex γ-ray spectra such as those produced by many unseparated fission products, it is unavoidable that some γ–ray lines from different isotopes will overlap. An example of this is the case of ^{147}Nd. Its 531.0 keV γ-ray with $T_{1/2}$=10.98 d overlaps with the 529.9 keV and $T_{1/2}$ = 20.83h γ–ray from ^{133}I. Even with our high-resolution HPGe detectors, these two lines are indistinguishable. Therefore, in order to obtain the correct ^{147}Nd activity, it is necessary to let the ^{133}I activity decay away, i.e., wait for about 200 h, and then record the true ^{147}Nd activity for a few weeks. Only then is it possible to extrapolate the ^{147}Nd decay curve back to time zero and obtain the initial ^{147}Nd activity of interest. This necessitates counting times that continue for a few weeks from the end of the production experiment. The associated decay curves and their extrapolations are illustrated in Fig.5. The yields of the γ-ray lines of interest were determined using the data-analysis software TV [12].

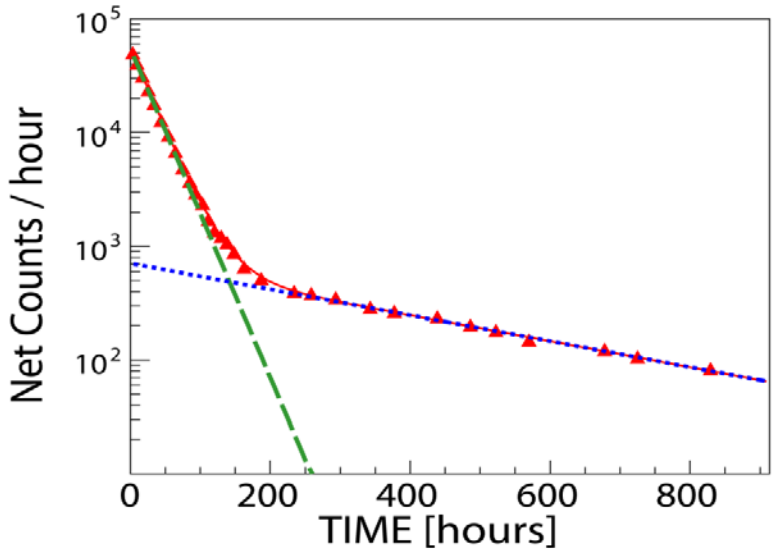

FIG. 5. (Color online) Decay of ^{133}I/^{147}Nd γ-ray yield (triangles) obtained at E_n = 8.9 MeV. The solid curve is a sum of two decaying exponentials. The dashed line represents the short-lived ^{133}I (E_γ = 529.9 keV; $T_{1/2}$ = 20.83 h). The dotted line characterizes the long-lived ^{147}Nd (E_γ = 531.0 keV; $T_{1/2}$ = 10.98 d).

Gamma-ray yield ratios are calculated by dividing the number of γ-ray events for a particular fission product by the yield (triangles) of a reference fission product. There are common factors, such as the number of target nuclei, and the neutron flux seen by these nuclei, that cancel in this ratio. It should be noted that these ratios are valuable, and their small uncertainties are important for testing model calculations. However, the interpretation of these ratios may not provide conclusive information about the energy dependence of the FPY itself, since the yield of both fission products may vary with energy in different ways. For this reason, the absolute γ-ray yields are normalized to the total number of fissions recorded in the dual-fission chamber in which the thick actinide target was irradiated. After applying finite geometry corrections based on Monte-Carlo simulations, the two fission chamber counts are averaged to yield the number of fissions per reference foil mass. By scaling this number up by the mass of the thick actinide target, the total number of fissions that occurred in the thick target during the course of irradiation was determined.

III. ANALYSIS

This section describes how the γ-ray and fission-chamber analyses were done to determine the absolute FPYs. It also briefly discusses the corrections applied to the FPY data.

III. A. Gamma-ray analysis

For the most prevalent cases for which the life time of the product being analyzed is long compared to its precursors, the cumulative number of fission product atoms, $N(^AZ)$, produced in the thick target at the end of the irradiation is given by

$$N(^AZ) = N_{tgt} * FPY(^AZ) * \sigma_f * \phi_{n,tgt} * (1-e(-\lambda t_{irr}))/\lambda \text{ ,} \quad (1)$$

where $FPY(^AZ)$ is the cumulative fission product yield for the ^AZ fission product, and λ is the decay constant ($=\ln 2/T_{1/2}$) for that isotope. The quantity N_{tgt} is the number of target nuclei, σ_f is the fission cross section, and $\phi_{n,tgt}$ is the neutron flux at the target position. The last term in Eq. (1) reduces to t_{irr} in the limit that the half-life time $T_{1/2}$ is much longer than the irradiation time t_{irr}.

The number of fission product atoms produced at the end of the irradiation is obtained from the number of γ-rays for that particular isotope measured in our HPGe detector after the irradiation, and is given by

$$N(^{A}Z) = N_{\gamma ct} / [C_i * \varepsilon_\gamma * I_\gamma * e(-\lambda t_d) * (1-e(-\lambda t_{ct}))], \quad (2)$$

where $N_{\gamma ct}$ is the net number of γ-ray counts recorded in the photo-peak, C_i are correction factors described below, ε_γ is the photo-peak efficiency of the detector at the requisite energy, I_γ is the γ-ray intensity, $e(-\lambda t_d)$ is the decay factor with t_d being the time from the end of the irradiation to the start of the counting, and $(1-e(-\lambda t_{ct}))$ gives the fraction of atoms that decay during the counting time t_{ct}.

By combining equations 1 and 2, an expression for $N_{\gamma ct}$ can be obtained:

$$N_{\gamma ct} = C_i * FPY(^{A}Z) * N_{tgt} * \sigma_f * \phi_{n,tgt} * \varepsilon_\gamma * I_\gamma * e(-\lambda t_d) * (1-e(-\lambda t_{ct})) * (1-e(-\lambda t_{irr}))/\lambda. \quad (3)$$

In the final analysis corrections (C_i) were made for: (1) γ-ray attenuation in the thick target (i.e., self-absorption); (2) differences between the size of the calibration sources, typically 5 mm in diameter compared to the target and reference foil diameter of 12.7 mm; (3) data-acquisition dead time of the computer collecting the γ-ray data; and (4) summing corrections. Monte-Carlo calculations were performed to address points (1), (2), and (4). The self-absorption corrections range from 1% to 18% depending on the γ-ray energy. The source-target geometry corrections were typically 1-2%. As mentioned above, the dead time associated with the γ-ray counting of the ^{239}Pu target was 11%, while for ^{235}U and ^{238}U dead-time corrections of 1% or less were applied. The dead-time corrections applied for the efficiency measurements of the HPGe detectors were typically below 3%. The cascade summing correction includes the decay scheme characteristics and the peak and total detection efficiencies. The largest summing correction of 3% was applied for the ^{99}Mo isotope, while for the other fission products this correction was 1% or less.

To test the adequacy of our dead-time correction procedures the high-activity ^{239}Pu target was counted in the presence of a ^{137}Cs source (661 keV γ-rays) of known activity. Even at this relativity high dead time (~ 11%) the pile-up and summing effects were compensated for correctly by our electronics and analysis procedures.

III. B. Fission product yield determination

The number of fissions that occur in our thick production target is determined by scaling the number of fission counts N_{fct} recorded in the two reference foils during irradiation by the mass ratio of the thick/reference foils. Minor corrections to this ratio are applied dealing with geometrical, kinematical, and focusing issues associated with the specific reaction.

The number of fissions N_{fct} recorded in one of the dual fission chambers relevant to a specific isotope is given by

$$N_{fct} = N_{ref} * \sigma_f * \Phi_{n,ref} * \varepsilon_f * t_{irr}, \quad (4)$$

where N_{ref} is the number of atoms in the reference foil, ε_f is the efficiency of the fission chamber, t_{irr} is the irradiation time, $\Phi_{n,ref}$ is the neutron flux at the reference foil position, σ_f is the fission cross section at the neutron energy of interest, λ is the decay constant, and t_{irr} is the irradiation time.

Forming the ratio $N_{\gamma ct}/N_{fct}$ using Eqs. (3) and (4) and solving for FPY(^{A}Z) one obtains:

$$FPY(^{A}Z) = (N_{\gamma ct}/N_{fct})*(N_{ref}/N_{tgt})*(\Phi_{n,ref}/\Phi_{n,tgt})*(\varepsilon_f/\varepsilon_\gamma)*\lambda* t_{irr}*[I_\gamma*(1-e(-\lambda t_{irr})*e(-\lambda t_d)*(1-e(-\lambda t_{ct}))]^{-1} \quad (5)$$

As can be seen, and stated earlier, this approach eliminates the need to know the fission cross section. However, Eq. 5 still requires information on several quantities:

(1) $\Phi_{n,ref}/\Phi_{n,tgt}$ - Due to the finite geometry of the experimental setup, the neutron flux at the target and reference foil(s) is somewhat different. This is due to the slightly different solid angles subtended by the three foils with respect to the neutron source. Taking simply the average of the upstream FC2 and downstream FC1 fission chamber counts could result in a 1% error. Monte-Carlo simulations were used to predict the neutron flux at the target position from the measured neutron flux ratio obtained from the two reference foils. Here, the differential cross section of the $^{2}H(d,n)^{3}H$ reaction, and the neutron attenuation between FC2 and FC1 were taken into account. Due to our close geometry the difference in neutron flux between the target position and the reference foil position in FC2 was found to be 10%.

(2) $\varepsilon_f/\varepsilon$ – A small correction to the dual-fission chamber efficiencies is caused by the center-of-mass motion of the fission fragments. The associated correction of 0.8% decreases the efficiency of the upstream FC2 fission chamber and increases the efficiency of the downstream FC1 by this amount.

(3) N_{ref}/N_{tgt} - A small change in the effective fission cross section is due to the isotopic content of the target relative to that of the reference foil. The associated corrections are less than 1% with the exception of the ^{235}U target, where the effective fission cross-section correction is 2.6%, due to the lower (93.3 %) isotopic enrichment of this target.

(4) The dead-time correction for the data-acquisition system used to records the number of fission events was less than 1%.

(5) The neutron beam is not mono-energetic and there is a very small component of off-energy neutrons that induce fission in our system. The procedure we use to correct for these events is described below.

IV. OFF- ENERGY NEUTRON CORRECTION

Off-energy neutron corrections would not be required if the FPYs were energy independent. However, the work of Glendenin *et al*. [13] on ^{235}U, Nagy *et al*. [14] on ^{238}U and Gindler *et al*. on ^{239}Pu [15] below incident neutron energies of 8 MeV clearly showed that the FPYs for most isotopes are indeed energy dependent.

From our TOF measurements we know the spectral shape of the total neutron energy range. Therefore, to the extent that the FPYs are known at these varying energies it is possible to simple remove their contribution and generate the "true" FPY at the energy of interest. By weighting the measured FPYs by their relative off-energy neutron contributions we can correct our data and transform them into FPYs at our primary energy of 8.9 MeV. The corrections are typically less than 0.5% and can be applied with an uncertainty of ~30%, resulting in a total contributed error for off-energy neutrons of less than 0.2%.

V. RESULTS

The triangles in Fig. 6 show our results for the yield of eight fission products ranging from ^{92}Sr to ^{147}Nd obtained from fission of ^{235}U with 8.9 MeV neutrons in comparison to the data of Glendenin *et al*. (dots) [13] at lower energies and those of Mac Innes *et al*. (squares) [16] and Laurec *et al*. (stars) [17] at 14.1 and 14.7 MeV, respectively. Typically, the FPYs vary between approximately 0.5% for ^{105}Ru and 6% for ^{140}Ba. Our data support the negative slope of the energy dependence previously observed for the high-yield fission products ^{97}Zr, ^{99}Mo, ^{140}Ba, ^{143}Ce and ^{147}Nd. The situation for ^{132}Te and ^{105}Ru is uncertain. While the previous data suggest no energy dependence for ^{132}Te up to 9 MeV, our datum at 9 MeV is even lower than the results of Laurec *et al*. and Mac Innes *et al*. in the 14 MeV energy range. For the low-yield fission product ^{105}Ru our datum is inconsistent with the trend of the previous data, which indicate a positive slope. Data in the 14 MeV energy regions are not available for ^{105}Ru to draw further conclusions.

Turning now to the FPYs obtained for ^{238}U, our data (triangles) are presented in Fig. 7 for eight fission products ranging from ^{92}Sr to ^{147}Nd in comparison to the data of Nagy *et al*. (dots) [14] at lower energies and those of Mac Innes *et al*. (squares) [16] and Laurec *et al*. (stars) [17] at 14.1 and 14.7 MeV, respectively. We notice that for ^{238}U the measured FPYs are all within the 3 to 6% range, except for ^{105}Ru and ^{147}Nd. Our result for ^{105}Ru is below the trend of the previously existing data. Our data for ^{147}Nd indicate that this fission fragment exhibits a negative slope between 9 and 15 MeV. The present data at 8.9 MeV support the approximately energy-independent FPY results for ^{92}Sr, ^{97}Zr, ^{99}Mo, ^{132}Te, ^{140}Ba and ^{143}Ce, and the negative slope previously observed for ^{105}Ru.

Finally, the FPY data (triangles) obtained for the fission of ^{239}Pu with 8.9 MeV neutrons are compared in Fig. 8 to the data of Gindler *et al*. (dots) [15] at lower energies and those of Mac Innes *et al*. (squares) [16] and Laurec *et al*. (stars) [17] at 14.1 and 14.7 MeV, respectively. The yield for the same isotopes as those shown in Fig. 7 is displayed, ranging from 3 to 6%. While

the previous data below 8 MeV hardly indicate any energy dependence of the FPYs, the inclusion of the present data and those available in the 14 MeV energy regions definitely suggests a negative slope at higher energies, except for ^{92}Sr for which data are not available near 14 MeV.

Numerical results for the FPYs in neutron-induced fission of ^{235}U, ^{238}U and ^{239}Pu at E_n=8.9 MeV are shown in Tables IV-VI. The FPYs are given in the 2nd column, while the 3rd column is the absolute uncertainty associated with the FPY value. The 4th column represents the reduced error by combining in quadrature the uncertainties associated with the HPGe detector efficiency, fission chamber counts and decay time. It is often of interest to present FPY ratios with respect to a high-yield fission fragment. In the past, ^{99}Mo and ^{140}Ba were used as reference standards. Following this tradition, the right-hand side of Tables IV-VI provide this ratio and its uncertainties, normalized to ^{99}Mo (columns 5 to 7) and ^{140}Ba (columns 8 to 10), respectively.

As can be seen from Figs. 6, 7 and 8, the total uncertainty obtained in the present work is comparable or smaller than that reported for previous FPY experiments. The uncertainty budget is summarized in Table VII.

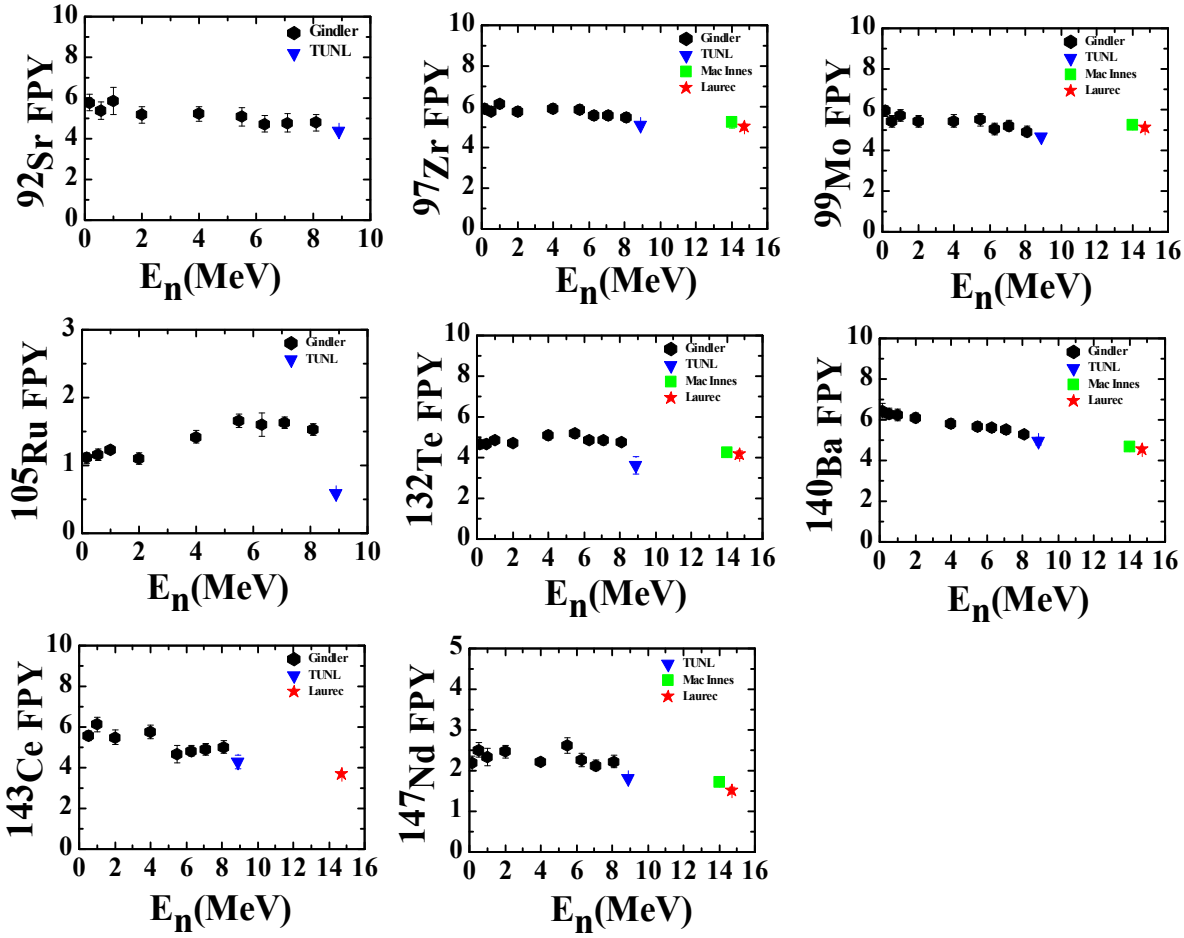

FIG. 6 (Color online) Energy dependence of fission product yields obtained in fission of ^{235}U with monoenergetic neutrons. The present datum (triangle) at 8.9 MeV is compared to the data (dots) of Glendenin *et al.* [13].

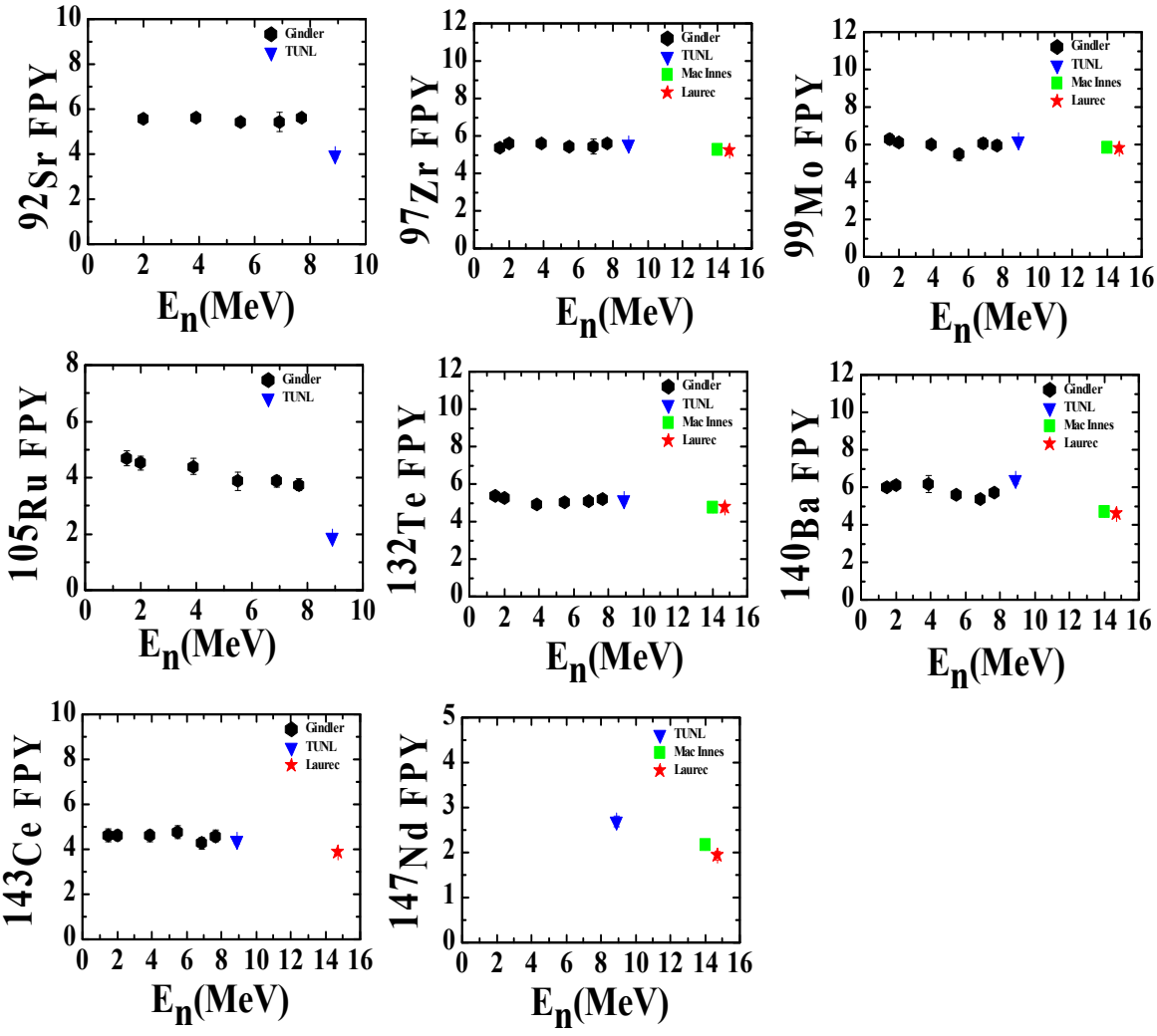

FIG. 7. (Color online) Energy dependence of fission product yields obtained in fission of ^{238}U with monoenergetic neutrons. The present datum (triangle) at 8.9 MeV is compared to the data (dots) of Nagy *et al.* [14].

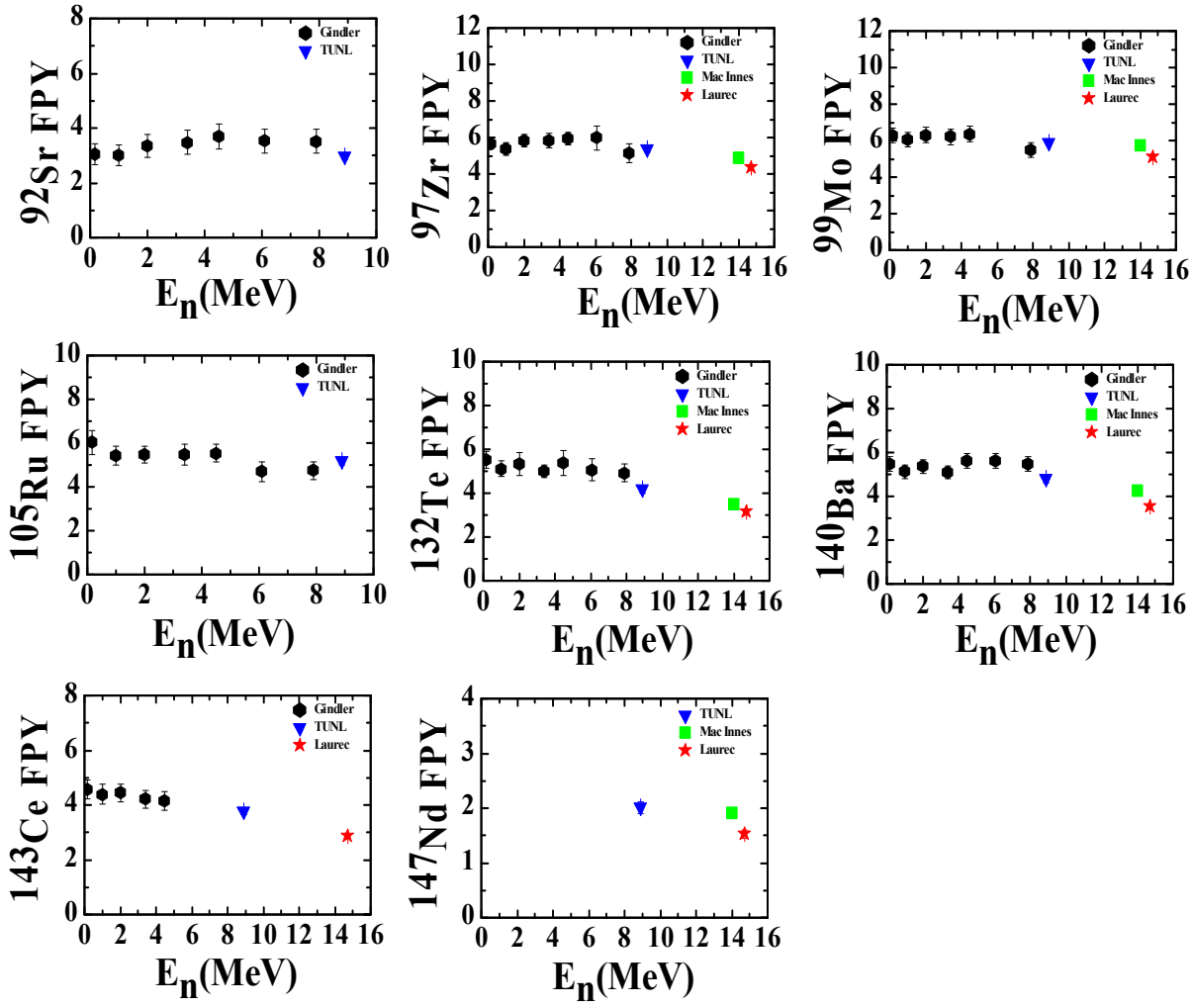

FIG. 8. (Color online) Energy dependence of fission product yields obtained in fission of ^{239}Pu with monoenergetic neutrons. The present datum (triangle) at 8.9 MeV is compared to the data (dots) of Gindler *et al.* [15].

Table IV. Fission product yield results obtained from neutron induced fission of ^{235}U at E_n=8.9 MeV.

^{235}U	FPY	Rel. Error	Abs. Error	FPY Ratio to ^{99}Mo	Rel. Error	Abs. Error	FPY Ratio to ^{140}Ba	Rel. Error	Total Error
^{92}Sr	4.38%	0.07%	0.31%	0.934	0.013	0.069	0.882	0.036	0.071
^{97}Zr	5.11%	0.11%	0.15%	1.089	0.008	0.039	1.029	0.016	0.048
^{99}Mo	4.69%	0.10%	0.16%	-	-	-	0.945	0.014	0.048
^{105}Ru	0.58%	0.02%	0.02%	0.123	0.003	0.005	0.116	0.003	0.006

^{132}Te	3.61%	0.43%	0.45%	0.771	0.109	0.098	0.728	0.079	0.095
^{140}Ba	4.96%	0.20%	0.23%	1.059	0.016	0.053	-	-	-
^{143}Ce	4.29%	0.35%	0.36%	0.916	0.070	0.080	0.865	0.048	0.080
^{147}Nd	1.81%	0.02%	0.05%	0.386	0.005	0.014	0.364	0.004	0.017

Table V. Fission product yield results obtained from neutron induced fission of ^{238}U at E_n=8.9 MeV.

^{238}U	**FPY**	**Rel. Error**	**Abs. Error**	**FPY Ratio to ^{99}Mo**	**Rel. Error**	**Abs. Error**	**FPY Ratio to ^{140}Ba**	**Rel. Error**	**Total Error**
^{92}Sr	3.94%	0.11%	0.31%	0.640	0.013	0.047	0.618	0.014	0.044
^{97}Zr	5.52%	0.14%	0.21%	0.897	0.016	0.024	0.866	0.012	0.019
^{99}Mo	6.16%	0.15%	0.28%	-	-	-	0.966	0.020	0.031
^{105}Ru	1.85%	0.05%	0.08%	0.300	0.007	0.010	0.290	0.006	0.008
^{132}Te	5.12%	0.15%	0.27%	0.831	0.021	0.038	0.803	0.017	0.034
^{140}Ba	6.38%	0.18%	0.27%	1.035	0.021	0.033	-	-	-
^{143}Ce	4.39%	0.13%	0.19%	0.712	0.016	0.023	0.688	0.013	0.020
^{147}Nd	2.69%	0.12%	0.15%	0.437	0.017	0.022	0.422	0.000	0.020

Table VI. Fission product yield results obtained from neutron induced fission of ^{239}Pu at E_n=8.9 MeV.

^{239}Pu	**FPY**	**Rel. Error**	**Abs. Error**	**FPY Ratio to ^{99}Mo**	**Rel. Error**	**Abs. Error**	**FPY Ratio to ^{140}Ba**	**Rel. Error**	**Total Error**
^{92}Sr	2.96%	0.09%	0.27%	0.501	0.008	0.038	0.617	0.021	0.047
^{97}Zr	5.36%	0.17%	0.34%	0.909	0.009	0.035	1.120	0.022	0.043
^{99}Mo	5.90%	0.13%	0.39%	-	-	-	1.233	0.025	0.053
^{105}Ru	5.18%	0.16%	0.34%	0.879	0.010	0.035	1.083	0.022	0.044
^{132}Te	4.17%	0.17%	0.32%	0.708	0.029	0.041	0.872	0.034	0.051
^{133}I	6.40%	0.21%	0.44%	1.086	0.013	0.052	1.338	0.023	0.064
^{140}Ba	4.79%	0.17%	0.32%	0.811	0.016	0.035	1.000	0.024	0.043
^{143}Ce	3.78%	0.12%	0.24%	0.640	0.015	0.026	0.789	0.021	0.032
^{147}Nd	2.01%	0.10%	0.22%	0.340	0.013	0.033	0.419	0.000	0.041

Table VII. Error analyses (%) for ^{235,238}U and ^{239}Pu at 8.9 MeV.

Error source	**^{235}U**	**^{238}U**	**^{239}Pu**
γ counts	0.18-2.1	0.36-3.5	0.37-3.0
Efficiency of HPGe detector (ε_γ)	0.51-3.79	0.56-1.60	1.85-3.30
Summing correction	0.2-3.0	0.2-3.0	0.2-3.0
FC2(FC1) cts.	0.088	0.130	0.332
Target mass FC2 (FC1)	8.96e-03	1.35e-04	0.043

Target diameter	0.404	0.403	0.403
Efficiency of fission chamber (ε_f)	1.53	1.50	2.28
Fission total (avg FC2+FC1)	2.0	2.16	2.20
Breakup neutrons	0.2	0.2	0.2
FPY total (reduced)	1.3-4.1	2.3-4.4	2.1-4.0

VI. CONCLUSIONS

The new experimental technique and associated analysis procedures used in the present work provide high-accuracy results for the absolute fission rate per nucleus and the absolute fission product yields for neutron-induced fission of ^{235}U, ^{238}U and ^{239}Pu at E_n=8.9 MeV. This experiment focused on eight FPYs between ^{92}Sr and ^{147}Nd. In the cases for which comparison to existing data is possible, the present FPYs follow in general the energy dependence suggested by previous measurements at lower energies as well as those in the 14 MeV energy regions. The present data are the first FPY results for ^{238}U and ^{239}Pu between 8 and 14 MeV. For ^{238}U additional data are needed in this energy range to support the conjecture of a negative slope for the energy dependence of the FPYs, as typically observed for ^{235}U and ^{239}Pu in this energy range. Such measurements are planned for the future, as well as measurements below 8 MeV to obtain a comprehensive set of FPY data to accurately determine their energy dependence.

ACKNOWLEDGEMENTS

We wish to thank M.B. Chadwick (LANL) for his insight and support for the present measurements. This work was performed under the auspices of U.S. Department of Energy at Duke University and Triangle Universities and Nuclear Laboratory through NNSA, Stewardship Science Academic Alliances Program Grant No. DE-FG52-09NA29465, DE-FG52-09NA29448 and at Los Alamos National Laboratory operated by the Los Alamos National Security, LLC under Contract No. DE-AC52 06NA25396 and at Lawrence Livermore National Laboratory operated by the Lawrence Livermore National Security, LLC under Contract No. DE-AC52-07NA27344.

1. O. Hahn and F. Strassmann, Naturwissenschaften **27**, 11 (1939).
2. R. Vandenbosch and J.R. Huizenga, Nuclear Fission, Academic, New York, 1973.
3. C. Bhatia *et al.,* Nucl. Instr. & Methods A **757**(1), 7 (2014).
4. D.W. Glasgow *et al.,* Nucl. Instr. & Methods **114**, 541 (1974).
5. G. Dietze and H. Klein, Technical Report PTB-ND-22, Physikalisch Technische Bundesanstalt, Braunschweig, Germany, 1982.
6. D.E. Gonzalez Trotter, F.S. Salinas Meneses, W. Tornow, A.S. Crowell, C.R. Howell, D. Schmidt and R.L. Walter, Nucl. Instr. Methods in Physics Research Section A **599**, 234 (2009).

7. H. Liskien and A. Paulsen, Nucl. Data Tables **11**, 569 (1973).
8. J. Grundl *et al.*, Nucl. Technol., **25**, 237 (1975).
9. http://www.canberra.com/products/radiochemistry_lab/genie-2000-software.asp
10. https://www-nds.iaea.org/exfor/endf.htm
11. Table of Radionuclides. http://www.nucleide.org/DDEP_WG/DDEPdata.htm
12. J. Theuerkauf *et al.*, *Computer code TV*, Technical report, Institute for Nuclear Physics, University of Cologne (1993).
13. L.E. Glendenin *et al.*, Phys. Rev**.** C **24**(6), 2600 (1981)**.**
14. S. Nagy *et al.*, Phys. Rev**.** C **17**(1), 163 (1978)**.**
15. J.E. Gindler *et al.*, Phys. Rev. C **27**, 2058 (1983).
16. M. Mac Innes, M.B. Chadwick, and T. Kawano, Nuclear Data Sheets **112**, 3135 (2011).
17. J. Laurec *et al.*, Nucl. Data Sheets **111**, 2965 (2010).